Atmospheric radiative equilibria in a simple column model *

Zhao-Xin Li[1], Kayo Ide[2], Hervé Le Treut[1], Michael Ghil[2]

(1) Laboratoire de Météorologie Dynamique du CNRS, Ecole Normale Supérieure, 24 rue Lhomond, 75231 Paris cedex 05, France

(2) Department of Atmospheric Sciences and Institute of Geophysics and Planetary Physics, University of California, Los Angeles, California 90095-1565

* Preliminary results of this work were presented at the First and Third UCLA – University of Tokyo Workshops, November 1993, Los Angeles, and December 1995, Honolulu, Hawaii California.

Correspondence to: Z.-X. Li

— —

Laboratoire de Météorologie Dynamique du CNRS
24 rue Lhomond, 75231 PARIS cedex 05, France
Fax:(33) (1) 43 36 83 92, E-mail: li@lmd.ens.fr

Revised version, November 1996
Climate Dynamics

Abstract. An analytic radiative-equilibrium model is formulated where both short- and longwave radiation are treated as two-stream (down- and upward) fluxes. An equilibrium state is defined in the model by the vertical temperature profile. The sensitivity of any such state to the model atmosphere's optical properties is formulated analytically. As an example, this general formulation is applied to a single-column 11-layer model, and the model's optical parameters are obtained from a detailed radiative parameterization of a general circulation model. The resulting simple column model is then used to study changes in the earth-atmosphere system's radiative equilibrium and, in particular, to infer the role of greenhouse trace gases, water vapor and aerosols in modifying the vertical temperature profile. Multiple equilibria appear when a positive surface-albedo feedback is introduced, and their stability is studied. The vertical structure of the radiative fluxes (both short- and longwave) is substantially modified as the temperature profile changes from one equilibrium to another. These equilibria and their stability are compared to those that appear in so-called energy-balance models, which heretofore have ignored the details of the vertical temperature and radiation profiles.

1 Introduction and motivation

Radiative equilibrium determines, to zeroth order, the Earth's climate. Energy-balance models (EBMs: Budyko 1969; Sellers 1969) are based on the net surface radiation at each latitude being redistributed by simple diffusive heat transfer between latitude belts to yield an equilibrium dependence of temperature on latitude. Analytic and semi-analytic versions of such EBMs (Held and Suarez 1974; North et al. 1981; Ghil and Childress 1987, Ch. 10) have permitted a thorough study of climate sensitivity to changes in atmospheric opacity, surface albedo and net radiative input at the top of the atmosphere. The understanding of the equilibrium sensitivity of the meridional temperature profile to various parameters has also led, in due course, to the formulation of nonequilibrium models that couple EBMs with ice-sheet flow models to study climatic variability on long time scales (Saltzman 1985; Ghil and Childress 1987, Ch. 11).

The meridional profile of zonally averaged surface air temperature is thus relatively well studied, in its equilibrium sensitivity and long-time changes. Analytic and semi-analytic EBMs have made a fundamental contribution to this understanding, by providing insight into a large number of observational data and numerical results obtained by using more detailed, three-dimensional general circulation models (GCMs). But temperature changes are actually sharpest — on average — with height. Furthermore, the atmosphere is a temperature-dependent filter, with spatially varying properties and numerous impurities, for the shortwave radiation traveling towards the Earth surface and the longwave radiation traveling back to space. The horizontally averaged temperature profile as a function of height is thus determined by and determines in turn radiative fluxes at all levels of the atmosphere. The most important "impurity" of the dry atmosphere is water vapor, followed by anthropogenic trace gases and aerosols.

One-dimensional models to study the atmosphere's variability in the vertical are called radiative-convective models (RCMs). Simple numerical RCMs have been formulated early in the development of modern, quantitative climate dynamics (Manabe and Strickler 1964; Manabe and Wetherald 1967) to explore the effects of water vapor, clouds, aerosols and trace gases (Schneider and Dickinson

1974; Ramanathan and Coakley 1978; Charlock and Sellers 1980) on radiative-convective equilibrium, as well as formulate and test parameterizations of these effects for use in GCMs. These models have grown into complex and realistic tools for the study of the atmosphere's vertical structure (Nakajima et al. 1992; Held et al. 1993; Renno et al. 1994a,b). Still, there is a need to understand more precisely the basic physics which underlies the results and to determine the relative role of various model features. One way to achieve this goal is to seek a minimal model, governed by the simplest set of equations that can describe the radiative-convective processes of greatest interest.

The work of Hu and Randall (1994) has also brought attention to possible oscillatory modes of the atmospheric vertical column, self-excited by the non-linear interactions among radiation, cumulus convection, and the surface fluxes of sensible heat and moisture. Complete, analytic understanding of radiative forcing and associated feedback effects appears essential to help explore coupled, oscillatory modes of the vertical profiles of temperature and water vapor, as well as the possibility of multiple equilibria (Renno 1994).

We build here a highly simplified model of an atmospheric vertical column. The model is simple enough so that the radiative processes can be studied by purely analytical methods. The present study is restricted to building a simple tool, to the verification of its basic properties, particularly in the case of radiative equilibrium, and to outlining the connections of this framework with convection. We hope that, by adding various proposed greenhouse-gas, water-vapor and other feedbacks, more complex and realistic stability properties of radiative-convective equilibrium can be explored.

There are many possible applications of a model as simple as the one presented here. For example, the increase in greenhouse-gas concentration represents, to first order, a purely radiative perturbation of the vertical atmospheric structure. It is interesting to know how much of the temperature response can be interpreted directly in terms of a radiative-equilibrium perturbation. Recent controversies concerning the feedback effects that amplify or reduce greenhouse-gas forcing point to the need for studying further the stability or instability of the radiative equilibrium.

In Section 2, the general formulation of the model is derived from basic principles, and the thermal equilibrium profile and its sensitivity to the variations of atmospheric properties are calculated; details of the sensitivity calculations appear in Appendix. In Section 3, we apply the general formulation to a special case where the atmosphere is divided into 11 layers and the atmospheric radiative properties are calculated from the radiative fluxes of a GCM. A temperature-dependent surface albedo is introduced in Section 4 and leads to the existence of multiple equilibria; their stability is computed. A summary and discussion of the results follow in Section 5.

2 The analytic model

The physical processes occurring in a vertical atmospheric column are the radiative transfer of solar and terrestrial fluxes, turbulent diffusion in the planetary boundary layer, moist convection, and phase changes of water. The horizontal and vertical transports by the large-scale circulation contribute also to the energy and water balance. Let us denote by R the net radiative flux, and by C the energy flux due to other processes. At equilibrium, we have:

$$R(T, \mu, q) + C(T, q) = 0, \tag{1}$$

where T is the atmosphere's temperature, μ are its optical properties, and q other atmospheric variables. All the variables in Eq.(1) — dependent (R and C) and independent (T, μ and q) — are vertical profiles. Clearly, C is dominated by convection and the most important variable besides temperature is relative humidity, hence the notation q.

Holding q constant, small changes in temperature δT and optical properties $\delta\mu$ about equilibrium are connected by the equation

$$\frac{\partial R}{\partial T}\delta T + \frac{\partial R}{\partial \mu}\delta\mu + \frac{\partial C}{\partial T}\delta T = 0. \tag{2}$$

The partial derivatives in (2) will become, after discretization of the profiles in the vertical, Jacobian matrices. At constant q and neglecting the last term, the sensitivity of T to μ is given by

$$\frac{\partial T}{\partial \mu} = -(\frac{\partial R}{\partial T})^{-1}\frac{\partial R}{\partial \mu}. \tag{3}$$

2.1 Radiative equilibrium

In our step-by-step approach to a complete analysis of RCMs, the present study concentrates on radiative equilibrium, so we neglect all other contributions except that of radiative transfer. Furthermore, the radiative transfer is treated through a simple two-stream approximation of down- and upward fluxes for both the short- and longwave radiation, respectively.

We discretize the radiative transfer equation for a grey-body atmosphere into n layers, neglecting convection C in Eq. (1) and keeping q constant. For $0 \leq i \leq n$, D_i is the downward and U_i the upward shortwave flux, while I_i is the downward and F_i the upward longwave flux (see Fig. 1). Each layer of our model is characterized by the following radiative properties: shortwave transmissivity τ_i, shortwave reflectivity ρ_i, and longwave transmissivity t_i. The shortwave reflectivity at the surface is denoted by ρ_0; this surface albedo ρ_0 will play a major role in Section 4. Note that the diffusion of the longwave radiation is neglected. Hence, in this simple model, R_i is represented by the difference of downward fluxes D_i and I_i and of upward fluxes U_i and F_i, while $\vec{\mu}_i = (t_i, \tau_i, \rho_i)$ is the vector of optical properties in each layer i.

Fig.1 near here

To be more explicit, the temperature of each atmospheric layer changes as a result of net energy absorption by the layer. When the equilibrium state is reached, the net flux of every layer must be zero:

$$D_i - D_{i-1} - (U_i - U_{i-1}) + I_i - I_{i-1} - (F_i - F_{i-1}) = 0; \quad i = 1, 2, ..., n; \tag{4}$$

for the surface, this reduces to:

$$D_0 - U_0 + I_0 - F_0 = 0. \tag{5}$$

The upward and downward fluxes are related to each other by

$$\begin{cases} D_n = S/4, \\ D_i = D_{i+1}\tau_{i+1} + U_i\rho_{i+1}, \quad i = n-1, ..., 1, 0; \\ U_0 = D_0\rho_0, \\ U_i = U_{i-1}\tau_i + D_i\rho_i, \quad i = 1, 2, ..., n; \\ F_0 = \sigma T_0^4, \\ F_i = F_{i-1}t_i + (1-t_i)\sigma T_i^4, \quad i = 1, 2, ..., n; \\ I_n = 0, \\ I_i = I_{i+1}t_{i+1} + (1-t_{i+1})\sigma T_{i+1}^4, \quad i = n-1, ..., 1, 0; \end{cases} \tag{6}$$

here σ is the Stefan-Boltzmann constant, T_0 is the surface temperature, T_1, T_2, ..., and T_n are the temperatures of each atmospheric layer, and S is the solar "constant". While in a vertically continuous, rather than discrete, formulation of (1) a discontinuity arises between the actual surface temperature $T(z{=}0)$ and the surface-air temperature $T(z{=}\epsilon)$, there is no inconsistency in our interpretation of T_0 in the discrete layer model (4)–(6) as the former. Note that Eqs. (4)–(6) form a linear system for the radiative fluxes D_i, U_i, I_i and F_i, as long as the optical properties $\vec{\mu}_i$ are assumed to be given. The only inhomogeneous term in this system is the downward flux at the top of the atmosphere, $S/4$. Thus all the fluxes in the model are proportional to the solar "constant" S.

Strictly speaking, Eq. (6) is true for monochromatic transfer. We can, however, define equivalent properties to treat the transfer of broad-band radiation (Morcrette 1991). This procedure is widely used in GCM radiation schemes to improve their computational performance. Otherwise, Eq. (6) is quite general in its description of the two-stream short- and longwave fluxes. It is only in determining the equation's $\vec{\mu}$-dependent coefficients from the vertical profiles $\vec{T}$ and $\vec{q}$ that additional complexities arise and RCMs differ from each other.

With the relations (6), we can write Eqs. (4) and (5) in matrix form:

$$\mathbf{K}\vec{Q} = -\vec{E}, \tag{7}$$

where the left-hand side (LHS) corresponds to longwave and the right-hand side (RHS) to shortwave fluxes. The coefficients of the LHS form an $(n{+}1)$-by-$(n{+}1)$ symmetric matrix $\mathbf{K}$, whose entries $k_{ij} = k_{ji}$ depend on the atmospheric longwave transmissivities t_i,

$$\begin{cases} k_{00} = -1, \\ k_{ii} = -2(1-t_i), \quad i = 1, 2, ..., n, \\ k_{01} = (1-t_1), \\ k_{0j} = (1-t_j) \prod_{l=1}^{l=j-1} t_l, \quad j = 2, 3, ..., n, \\ k_{i,i+1} = (1-t_i)(1-t_{i+1}), \quad i = 1, 2, ..., n, \\ k_{ij} = (1-t_i)(1-t_j) \prod_{l=i+1}^{l=j-1} t_l, \quad i = 1, 2, ..., n \ (j > i+1); \end{cases} \tag{8}$$

$\vec{Q}$ is the vector of Stefan-Boltzmann fluxes that are in one-to-one correspondence with the temperatures, $\vec{Q} = (\sigma T_0^4, \sigma T_1^4, ..., \sigma T_n^4)$, and $\vec{E}$ is a vector whose components can be expressed as functions of τ_i and ρ_i.

Most of the shortwave radiation that reaches the surface is absorbed by it, so the reflected energy is relatively small. To keep the model simple and analytical, we neglect the upward shortwave flux's second, downward reflection (off an atmospheric layer). This yields the elements of $\vec{E}$ as

$$\begin{cases} E_0 = S/4(1-\rho_0) \prod_{l=1}^{l=n} \tau_l, \\ E_i = S/4(\prod_{l=i+1}^{l=n} \tau_l)\{1 - \tau_i - \rho_i + \tau_i(1-\tau_i)[\sum_{l=0}^{l=i-1}(\rho_l \prod_{m=l+1}^{m=i-1} \tau_m^2)]\}, \quad i > 0. \end{cases} \tag{9}$$

The equilibrium state is obtained by solving system (7), to yield the temperature profile:

$$T_i = [(-\frac{1}{\sigma}\mathbf{K}^{-1}\vec{E})_i]^{1/4}. \tag{10}$$

The present model contains additional simplifying assumptions, such as the down- and upward transmissivities being equal in Eq. (6). While *in situ* measurements have shown this not to be so in an inhomogeneous medium, distinct transmissivities can easily be incorporated in subsequent, more realistic models, that will include convective terms as well. Likewise, the model's grey-body assumption of multiplicative transmittances, Eq. (8), is only true for monochromatic fluxes. The point of this paper is not to present a non-grey RCM more sophisticated than any in existence, but to illustrate with a simple, grey-body RCM how sensitivity can be studied exhaustively by analytic methods. Similar sensitivity calculations can then be implemented on much more realistic RCMs, at the forefront of research, by the use of semi-analytical or even theory-guided numerical methods (compare with the EBM situation, as described in Part IV of Ghil and Childress 1987).

2.2 Sensitivity of the equilibrium

The main advantage of the present formulation is that we can study analytically the effect of prescribed changes in atmospheric radiative properties on the temperature profile. The radiative transfer equation (7) can be rewritten as:

$$\vec{G}(\vec{T};\vec{t},\vec{\tau},\vec{\rho}) \equiv \mathbf{K}\vec{Q} + \vec{E} = \vec{0}. \tag{11}$$

At equilibrium $\vec{G}(\vec{T};\, \vec{t},\, \vec{\tau},\, \vec{\rho})$ is identically zero, a property which we use to differentiate not only the radiative fluxes, but also the temperature at a given level, with respect to the atmosphere's optical properties. The connection between Eqs. (11) and (1) is given by $\vec{\mu} = (t,\tau,\rho)$ and the neglect of C and q. In general, for a vertically discretized model, $\vec{G} = \vec{R} + \vec{C}$ and $\vec{\mu} = \vec{\mu}(\vec{T},\vec{q})$; to emphasize that we consider here the optical properties $\vec{\mu}$ of the atmosphere as given parameters, we separate between the variable $\vec{T}$ and the properties $\vec{\mu}$, as arguments of $\vec{G}$ (or $\vec{R}$), by a semi-colon.

To measure the displacement of the equilibrium profile $\vec{T}$ resulting from a change in longwave transmissivity $\vec{t}$, we apply the implicit function theorem to Eq. (11). Suppose that the small change in $\vec{t}$ is $\delta\vec{t}$ and, as a consequence, the temperature profile is modified by an amount $\delta\vec{T}$ to yield a new equilibrium profile $\vec{T} + \delta\vec{T}$. The resulting net change $\delta\vec{G}$ in $\vec{G}$ is zero:

$$\frac{\partial\vec{G}}{\partial\vec{t}}\delta\vec{t} + \frac{\partial\vec{G}}{\partial\vec{T}}\delta\vec{T} = \vec{0}. \tag{12}$$

This derivation is entirely analogous to that of Eq. (2) from Eq. (1).

Solving (12) for the sensitivity of $\vec{T}$ to $\vec{t}$ yields

$$\frac{\partial\vec{T}}{\partial\vec{t}} = -(\frac{\partial\vec{G}}{\partial\vec{T}})^{-1}(\frac{\partial\vec{G}}{\partial\vec{t}}). \tag{13}$$

Similar equations can be deduced for equilibrium-profile sensitivities with respect to $\vec{\tau}$ and $\vec{\rho}$. To obtain all three sensitivities, it is necessary to calculate the matrices $\partial\vec{G}/\partial\vec{T}$, $\partial\vec{G}/\partial\vec{t}$, $\partial\vec{G}/\partial\vec{\tau}$, and $\partial\vec{G}/\partial\vec{\rho}$, *i.e.*, the Jacobian derivatives of the vector function $\vec{G}$ with respect to the temperature, longwave transmissivity, shortwave transmissivity and shortwave reflectivity vectors.

The derivative of $\vec{G}$ with respect to the temperature forms a square $(n+1)$-by-$(n+1)$ matrix:

$$\begin{aligned}(\frac{\partial\vec{G}}{\partial\vec{T}})_{ij} &= \frac{\partial G_i}{\partial T_j} \\ &= \frac{\partial}{\partial T_j}\sum_{l=0}^{l=n} k_{il}\sigma T_l^4 = k_{ij}4\sigma T_j^3, \quad i=0,1,...,n, \quad j=0,1,...,n. \quad (14)\end{aligned}$$

Note that the partial differentiation here assumes, as already stated, that the coefficients k_{il} remain constant. Denoting by $\mathbf{W}$ the diagonal matrix with $W_{ii} = 4\sigma T_i^3$, we have immediately:

$$\frac{\partial\vec{G}}{\partial\vec{T}} = \mathbf{KW}, \quad (15)$$

and thus

$$(\frac{\partial\vec{G}}{\partial\vec{T}})^{-1} = \mathbf{W}^{-1}\mathbf{K}^{-1}. \quad (16)$$

The derivatives of $\vec{G}$ with respect to the longwave transmissivity $\vec{t}$, and shortwave transmissivity $\vec{\tau}$ and reflectivity $\vec{\rho}$ are given in the Appendix. The case in which any or all of these optical properties are allowed to depend on the temperature profile $\vec{T}$ can be treated in a similar manner by the chain rule for differentiation.

3 Application to a GCM's radiative equilibrium

With the formulation developed above, the equilibrium profile of temperature $\vec{T} \equiv (T_i)$ and its sensitivity can be obtained if the atmospheric fluxes, and hence radiative properties (t_i, τ_i, ρ_i) and surface albedo ρ_0, are given. In this section, we apply the formulation developed above to a case where the atmosphere is divided into 11 layers, and the radiative fluxes are obtained from a detailed radiative calculation.

3.1 The equilibrium profile

In order to obtain the atmosphere's optical properties within our model's framework, we can use an inverse formulation. Equation (6) can be applied to any set of temperatures and radiative fluxes, whether deduced from observations or from more detailed radiative transfer models. Here we use the results from a climate experiment with the Laboratoire de Météorologie Dynamique's GCM (Sadourny and Laval 1984). The emphasis is on trace gases rather than clouds, so we consider only the clear-sky case; the solar constant used in the experiment was $S = S_0 \equiv 1370$ Wm^{-2}. By performing a horizontal average over the whole globe and over the annual cycle, we obtain vertical profiles of temperature, water vapor and ozone (Table 1). The clear-sky radiative fluxes are then computed for every layer, using the scheme of Fouquart and Bonnel (1980) and Morcrette (1991). Tab.1 near here

It is important to recall that temperature and water-vapor profiles $\vec{T}$ and $\vec{q}$ in the GCM simulation — or in the real world — and, hence, the corresponding atmospheric optical properties $\vec{\mu}$, do not correspond to exact radiative equilibrium, especially not in the lower atmosphere. The profiles of temperature and radiative properties we obtain satisfy more closely Eq. (1) than (11). Similar approximations, however, are made in comparing RCM with GCM results and in tuning — implicitly or explicitly — the former to the latter, or to atmospheric observations. It is not even clear that a vertical column is, at any time, in radiative-convective equilibrium (compare Hu and Randall 1994 or Renno 1994). The purpose here, again, is to develop rigorous methodology for sensitivity studies and to apply it, in a self-consistent manner, to relatively simple cases.

The resulting profiles of t, τ and ρ (see Table 1) are of course consistent with well-known radiative transfer features, as implemented in the GCM, e.g., the atmosphere is relatively transparent for shortwave radiation and the vertical variations of transmissivity and reflectivity are small, especially for the present clear-sky case. The water-vapor content q_i decreases with altitude i and hence the longwave transmissivity t_i increases. The surface albedo is prescribed in the present section to be $\rho_0 = 0.3$; this corresponds to the global planetary albedo — averaged over both clear-sky and cloud-covered areas — rather than the observed surface albedo and thus helps ensure that the (net) absorbed shortwave radiation

(ASR) is correct in the clear-sky case. In the next section, we allow ρ_0 to vary as a function of T_0.

The model's equilibrium profile of temperature in this case is shown by the curve (a) in Fig. 2. The solid curve (labeled GCM) is the GCM's globally averaged profile and the curves (b) and (c) are two other equilibrium states described in Section 4. The surface temperature in our simple model is warmer than in the GCM, because vertical convective mixing is not present in our simple RCM. A pronounced tropopause does occur in our model at about the right altitude, while its temperature, as well as that of the middle atmosphere above it, are too high. Fig.1 near here

3.2 The equilibrium profile's sensitivity

Using the equations developed above and in Appendix, we calculate the sensitivity of the equilibrium temperature profile (a) in Fig. 1 to the variations of atmospheric radiative properties (t_i, τ_i, ρ_i). According to Eq. (12), the obtained sensitivity arises from the change in the fluxes due to the change in atmospheric optical properties being balanced by the changes in temperature profile necessary to conserve radiative equilibrium during this modification.

The upper panel of Table 2 shows the values of $\partial\vec{T}/\partial\vec{t}$, that is, the sensitivity of the equilibrium temperature with respect to the longwave transmissivity. Each row j in the panel represents the influence on the surface ($i = 0$) and the atmospheric ($1 \leq i \leq 11$) temperature T_i exerted by the variation in longwave transmissivity t_j of the given layer j. Each column i in the table measures the influence of the transmissivity t_j in different layers $1 \leq j \leq 11$ on the temperature T_i at the surface or in a given layer. Tab 2 near here

Somewhat surprising is that the temperature of a given layer does not depend on the transmissivity of the lower layers: the values are identically 0 below the diagonal line $i = j$. This is not a numerical artifact and can be easily proved in the case of a two-layer model where Eq. (7) yields that:

$$\sigma T_2^4 = \frac{E_0 + E_1}{1 + t_2} + \frac{E_2}{1 - t_2^2} \tag{17}$$

and hence T_2 does not depend on t_1.

This property is, indeed, inherent in radiative equilibrium. The physical reason is that when the transmissivity t_j of a layer is increased, its absorptivity and hence emissivity $\epsilon_j{=}1{-}t_j$ is decreased, so the increase of upward flux received from the lower layers is exactly cancelled by the decrease in the emission from the given layer. The proof (17) can be extended to the case of $n \geq 3$ levels by induction on n. More intuitively, consider the influence of t_j on the temperature T_i, with $i > j$. To do so, change the problem to a two-layer model with lower layer containing j and upper layer containing i. It is then straightforward to conclude that t_j does not influence T_i. This property will not hold for a model where the atmosphere's optical properties do depend on temperature and feedbacks between the former and the latter are allowed.

When the longwave transmissivity of a layer is increased, its greenhouse effect decreases, and the surface and all the layers below this layer are then cooled. The cooling effect is maximum just below the perturbed layer and decreases as one moves away from the perturbed layer. For the perturbed layer itself, its temperature decreases when it is in the troposphere (where the layers below are warmer), but increases when it is in the stratosphere (where the layer below is cooler). The middle-atmospheric warming is greatly enhanced due to the fact that the longwave emissivity $\epsilon_j{=}1{-}t_j$ of these upper layers to nearby space is decreased and the local loss of energy is diminished.

A CO_2-doubling is roughly equivalent to a decrease of 0.8% in the longwave transmissivity. The associated temperature change in the present model is shown Fig.3 near here in Fig. 3. It is clear that the purely radiative effects captured by our very simple, linear model explain one of the most important aspects of CO_2-doubling experiments using full GCMs: the stratosphere cools and the troposphere warms [*e.g.*, Schlesinger and Mitchell (1987)].

The middle panel of Table 2 shows the derivative of temperature with respect to the transmissivity of shortwave radiation. The main diagonal, $i = j$, is negative and strongly dominant in absolute values. Thus, if the shortwave transmissivity of a layer is increased, its own temperature is decreased by a large amount. This drop in temperature occurs because the shortwave absorption of that layer is substantially decreased. We also observe in this panel that the entries become positive and larger as we move away from the main diagonal toward the lower layers (upper-left corner), while they are negative and decrease in absolute value as we move toward the upper layers (lower-right corner). These two results can be explained as follows. The increase of shortwave transmissivity in a given layer allows more shortwave radiation to go through it and warm the lower layers and the surface, thus explaining the first result. The second result arises from the smaller effects of the surface and lower-layer warming on the upper layers.

Finally, the lower panel of Table 2 gives the sensitivity of the equilibrium temperature with respect to the reflectivity of shortwave radiation. When the system becomes more reflective, the absorbed energy diminishes and the temperature of all layers is decreased. The main diagonal in the figure is again strongly dominant, showing the importance of local radiative effects. The influence of the reflectivity perturbation diminishes away from the perturbed layer, both up- and downward. Sensitivity to both shortwave radiation parameters (middle and lower panels of Table 2) has a maximum for the uppermost levels (upper-right corner of both tables).

The diagonally dominant structure of the middle and lower panels of Table 2 — with the largest diagonal elements just above the tropopause — shows that, when increasing the shortwave transmissivity or reflectivity, the static stability of the lower atmosphere is decreased and that of the middle atmosphere is increased. These static stability changes can, in turn, influence the atmospheric radiative properties through changes in clouds or water vapor. Of course the sign and magnitude of these radiative-convective feedbacks will depend upon how the clouds or water vapor change. For a given convective parameterization $C = C(T, q)$ in Eq. (1), they can be determined analytically by the methodology outlined here (see Section 5.2 below).

Table 3 shows the sensitivity of surface and atmospheric temperatures with respect to the surface albedo. The temperatures clearly decrease when the surface albedo is enhanced. As remarked by Manabe and Wetherald (1967), the influence diminishes with increasing altitude and hence the atmosphere's static stability Tab 3 near here increases. In Section 4 below, we pursue this issue further by considering a temperature-dependent surface albedo.

4 Surface-albedo feedback

Allowing surface albedo to increase with decreasing temperature (Budyko 1969; Sellers 1969) — due to the appearance of snow and ice at low temperatures — induces a positive feedback into the climate system which counteracts the negative feedback of the outgoing longwave radiation (OLR). In many EBMs, this leads to the existence of multiple equilibria (Held and Suarez 1974; North 1975; Ghil 1976) and can contribute to the presence of self-sustained climatic oscillations when coupling such EBMs to ice-mass balance models. Oscillatory paleoclimate models (Källén et al. 1979; Ghil and Le Treut 1981; Saltzman 1985) provide tentative explanations for the large amplitude of glacial-interglacial cycles during the Quaternary, when subject to quasi-periodic insolation forcing due to changes in the Earth orbit on these time scales (Le Treut and Ghil 1983; Ghil and Childress 1987, Ch. 12).

In these EBMs and coupled paleoclimate models, the vertical structure of the atmosphere has been given short shrift, and the energy balance typically expressed as a balance at the surface,

$$m(T_0)\sigma T_0^4 = \frac{S}{4}[1 - \rho_p(T_0)]. \tag{18}$$

In Eq. (18), the role of the vertical structure is only taken into account by including the "greyness" or "greenhouse" factor $m(T_0)$ with $m \approx 0.5$ (Sellers 1969; Ghil 1976), and by replacing a realistic surface albedo ρ_0 by a planetary-albedo value $\rho_p = \rho_0(T_0)$. The possibly crucial role of the atmosphere's vertical structure in amplifying any climatic change through water vapor or cloud feedbacks is however increasingly recognized. All changes in the longwave component of the Earth radiation budget turn out to be intimately associated with changes in the vertical temperature lapse rate (Bony et al. 1995). It is clear, of course, that the atmosphere's vertical structure is never in radiative equilibrium. However the radiative transfer equation serves as a backbone for our insights into this structure and its variations; we need, therefore, to gain a complete understanding for this equation's solution space before we consider other vertical-transport processes such as convection. This is the avenue we pursue in the present section.

4.1 Model formulation

Representing both the short- and longwave radiative fluxes at the top of the atmosphere as a function of surface temperature, according to Eq. (18), provides a convenient "first crack" at studying the Earth radiative equilibrium. The intersection of the two curves — the OLR on the LHS of Eq. (18) and the ASR on the RHS, when plotted against T_0 — determines the equilibrium states and their stability follows easily from the slope of the difference between the two curves at the intersection points (Ghil and Childress 1987, Ch. 10). Using surface temperature T_0 as an indicator of a given climate is also natural because the atmosphere stores little energy and hence the ground or ocean temperature is the best measure of the energy absorbed by the Earth.

Surface albedo is a function of snow- and sea-ice-cover extent on short time scales of months-to-decades. Dependence on the presence and nature of vegetation (e.g., Chalita and Le Treut 1994) and on sea state is also known to exist, but harder to take into account. In many zero- or one-dimensional EBMs, the surface albedo is parameterized in a very simple manner, by letting the cryospheric cover be a function of surface temperature alone. When the surface temperature is smaller than a critical value T_l, the surface is ice-covered and the surface albedo is prescribed to have a constant, high value, α_M; when the surface temperature is larger than a critical value T_u, the surface is ice-free, and the surface albedo is prescribed to have a constant, low value, α_m; linear interpolation is used between these two extreme situations (Sellers 1969; Ghil 1976) or a jump between the two is allowed (Budyko 1969; Held and Suarez 1974; North 1975).

To study the behavior of our model in the presence of surface-albedo changes $\rho_0 = \rho_0(T_0)$, we follow Sellers (1969) and Ghil (1976):

$$\rho_0 = \begin{cases} \alpha_M & \text{for } T_0 \leq T_l; \\ \alpha_m & \text{for } T_0 \geq T_u; \\ \alpha_M + \frac{T_0 - T_l}{T_u - T_l}(\alpha_m - \alpha_M) & \text{for } T_l < T_0 < T_u. \end{cases} \tag{19}$$

In the EBM literature there has been considerable discussion on the "best" values of T_l, T_u, α_M and α_m [see, for instance, Ghil (1984) for a review]. In this exploratory study, we take $T_l = 258$K, $T_u = 288$K, $\alpha_M = 0.9$ and $\alpha_m = 0.3$. Unlike in EBMs, the albedo values α_m and α_M in Eq. (19) are truly meant to refer to surface, and not to an integrated planetary albedo.

In EBMs the planetary albedo ρ_p is usually identified with the surface albedo ρ_0. But when considering the atmosphere's vertical structure, as in RCMs, the planetary albedo depends not only upon the surface albedo, but also upon the back-scattering of the atmosphere. As a consequence, the planetary albedo increases more slowly than the surface albedo does: $\partial\rho_p/\partial\rho_0 < 1$. Likewise, the planetary albedo may remain substantial even for low surface albedo. The corresponding relation between surface and planetary albedo is given in Fig. 4 for our simple model (solid curve). The straight bisector (dotted) indicates the relation between surface albedo and planetary albedo when there is no atmosphere. In the real atmosphere, optical properties can also change as the temperature profile changes, and this relation can thus become more complicated. Fig.4 near here

The OLR in EBMs is often related to the surface temperature by using linear regression between observed emission to space and surface temperatures (Budyko 1969; Held and Suarez 1974; North 1975). This approach does include some contribution of changes in temperature lapse rate, since the outgoing radiation should obey the Stefan-Boltzmann law, modified empirically by a greyness factor $m(T_0)\sigma T_0^4$ (Sellers 1969; Ghil 1976) when the vertical structure is neglected. But this lapse-rate effect is in fact adjusted to fit geographical variations within the present climate conditions. It means that in EBMs it is assumed that the average temperature lapse rate is close to that of the polar regions when the climate of the Earth becomes colder, and close to that of tropical regions when the temperature becomes warmer. This is bound to be wrong since, within a reasonable range of climate changes, on a time scale of months to decades, there will coexist regions of rising unstable air and subsiding stable air.

In our RCM, the OLR equals F_n and is no longer directly related to the surface temperature, but depends on the vertical stratification of the atmosphere as well. To obtain the relation between OLR and surface temperature, for comparison with EBMs, one needs to solve the radiative transfer equation, determine the vertical temperature distribution from Eq. (10), and compute the fluxes accordingly.

4.2 Multiple equilibria and their stability

To explore the model's behavior in response to changes in the solar constant, we compute first the surface albedo corresponding to a given surface temperature through Eq. (19), and then adjust the solar constant S to reach the equilibrium profile with that surface temperature. The resulting OLR curve is displayed in Fig. 5 (solid); breaks in the slope of this curve appear at the points T_l and T_u. Fig.5 near here
Also displayed in the figure are the curves used *a priori* by Crafoord and Källén (1978) and North et al. (1981) for OLR, $F = F(T_0)$, say: $F = 1.74(T_0 - 154)$ and $F = 2.09(T_0 - 273) + 203$ respectively.

The difference between the three curves in the figure gives a rough measure of the quantitative importance of the vertical temperature profile, even in such simple models. The slope of OLR against surface temperature T_0 for the interval between the slope breaks, $T_l < T_0 < T_u$, is smallest due to the change in the character of the dependence of ASR, and hence radiative equilibrium on surface temperature in this interval, as we shall see below.

Figure 6 displays the relation between the normalized solar constant, S/S_0, Fig.6 near here
and the surface temperature T_0. This curve (heavy solid in the figure) is obtained by using the same procedure as for Fig. 5. Three equilibrium profiles can exist for a large range of solar-constant values. The intersection point (a) between the heavy solid curve and the dotted vertical line for the present value of the solar constant $S/S_0 = 1$ corresponds to the present climate, the point (b) to a totally ice-covered Earth, often called "deep freeze" in the EBM literature, and the point (c) to an intermediate equilibrium. The corresponding temperature profiles are displayed in Fig. 2 (curves a, b and c).

The curve shown in Fig. 5 is closely related to the S-shaped bifurcation curve of global mean temperature vs. normalized solar constant S/S_0 in Ghil's (1976) one-dimensional EBM. This in turn is related to the curves of ice-margin position vs. solar constant in the Budyko-type models of Held and Suarez (1974) and North (1975); see for instance Table 10.1 and Section 10.2 in Ghil and Childress (1987).

Figure 7 displays the variations of shortwave and longwave radiative fluxes at the top of the atmosphere (ASR and OLR) as a function of the surface temperature. The combined information from Figs. 6 and 7 indicates that the change in slope of the model's OLR curve for the intermediate "climate" is due to the fact that the ASR's slope here is large and positive with respect to surface temperature (Fig. 7), while it is moderate and negative with respect to the implied solar constant (Fig. 6); the associated OLR adjusts as required to maintain radiative equilibrium over this surface temperature range. The three equilibria in Figs. 2 and 6 correspond to the three intersection points of ASR and OLR curves. If we increase or decrease the value of the solar constant, the ASR curve moves up- and downward in direct proportion to S and bifurcations take place when the intermediate solution coalesces with either the "present-day" solution or the "deep-freeze" one. Fig.7 near here

The stability of the three equilibria can be determined as follows. Let us consider first the intermediate solution at $T_0 = T_c$. If, for some reason, T_0 goes up slightly, then ρ_0 decreases, according to Eq. (19). This implies more shortwave radiation absorbed by the Earth-atmosphere system, which requires an increase in longwave emitted to maintain the radiative equilibrium. This, however, requires a further increase in surface temperature, and so on, leading to a runaway increase in T_0. A similar argument holds for an initialy small decrease in T_0 from the value T_c leading to a runaway decrease in surface temperature. Thus the intermediate equilibrium is unstable. In the same intuitive manner, we can show that the present-day and "deep-freeze" solutions are stable. Mathematically, we can define, recalling ASR $= D_n - U_n$ and OLR $= F_n$,

$$s \equiv \frac{\partial F_n}{\partial T_0} - \left(\frac{\partial D_n}{\partial T_0} - \frac{\partial U_n}{\partial T_0}\right). \tag{20}$$

If s is positive, then the equilibrium is stable; otherwise, it is unstable. The arguments are similar to those illustrated for zero-dimensional EBMs by Ghil and Childress (1987, Ch. 10). The presence of an unstable equilibrium separating two stable ones holds for spatially one- and higher-dimensional models as well, provided the model admits a variational principle with a continuously differentiable functional (Ghil 1976; North et al. 1979). This follows from the so-called "mountain-pass" lemma (Nirenberg 1981; Ghil and Childress 1987, p. 334).

5 Concluding remarks

5.1 Summary

We have developed an analytic model for radiative transfer using basic principles and prescribed fluxes, shortwave and longwave, from a GCM clear-sky radiation computation. Our purpose was to understand the atmosphere's thermal structure and to study its equilibrium sensitivity to different perturbations of radiative properties. The first-order partial differentiation described here is equivalent to considering prescribed perturbations in the atmosphere's optical properties and not allowing temperature changes to affect these perturbations in turn. It is interesting that such a simple computation provides an adequate explanation for many well-known features of climate response to changes in greenhouse-gas or aerosol concentrations, as well as in cloud cover, type or elevation (e.g. Stephens and Webster 1981; Charlock and Sellers 1980; Nakajima et al. 1992).

The main greenhouse-gas effect is to render the atmosphere more opaque to longwave radiation, i.e., to decrease atmospheric longwave transmissivity t. We find that, by decreasing t, the surface and the lower and middle troposphere are warmed, because more energy is trapped there, while the upper troposphere and stratosphere cool, because the energy lost there by longwave emission exceeds the trapping effect.

Our approach also accounts for other changes in atmospheric radiative properties which may occur due to aerosol loading, namely a decrease in shortwave transmissivity τ and an increase in shortwave reflectivity ρ. For a given layer, if the transmissivity for shortwave radiation τ is decreased, its equilibrium temperature increases, and so does that of the layers above it. But the lower layers and the surface are cooled since less shortwave radiation reaches them

If the atmospheric reflectivity for shortwave radiation ρ increases, the entire atmosphere gets colder, since more shortwave radiation is reflected to outer space. This cooling, however, is not homogeneous and the layer whose reflectivity is changed is most affected. The same is true for the warming due to a decrease in τ being strongest in the layer where the decrease occurs. The overall effect of aerosol concentrations increases is to cool the atmosphere's lower layers and the surface, while the effect on the upper layers is much smaller and can be of either sign, on balance.

Clouds, on the other hand, depending on their altitude and type, affect to various degrees all of the atmosphere's optical properties, $\vec{\mu} = (t, \tau, \rho)$. Therefore it is necessary to consider specific profiles of $\delta\mu$ as a function of vertical coordinate, whether height or pressure, in order to determine their effects on the layers where clouds are present, as well as on those above and below. At the same time, it would be interesting to apply the present model to a cloud-free planetary atmosphere, such as that of Mars, where carbon-dioxide loading, oscillates with the seasons and dust loading fluctuates episodically.

The consideration of atmospheric vertical structure modifies substantially the dependence of the short- and longwave radiation at the top of the atmosphere (ASR and OLR) on the surface albedo and surface temperature. As in many EBMs, we introduced a positive surface-albedo feedback and studied the resulting multiple equilibria. In the present analytic RCM, three equilibrium profiles can co-exist for a large range of solar-constant values. The three states correspond respectively to an ice-covered Earth, an ice-free one, and an intermediate equilibrium. The latter is unstable, while the former two are stable.

5.2 Discussion

These results are all due to linear sensitivity of the radiative-equilibrium temperature to changes in the atmosphere's optical properties. They are somewhat in the spirit of Cess's (1976) attempt at obtaining climate-sensitivity results from a zonal, rather than vertical climatology, or that of Stephens and Webster (1981) at studying the effect of cloud height on climate. Though the results are based on a particular GCM, the general formulation can be applied to any observation-based climatology or to other GCMs.

The next step, however, should be much more interesting. Armed with these linear results, one can proceed to extend the model by including, one at a time, various feedbacks between the temperature, humidity and radiative properties. Drastic changes in the sensitivity of the multiple radiative equilibria might result when nonlinear feedback mechanisms are included or, to the contrary, the present results might turn out to be robust.

Proceeding next to coupled models, oscillatory or chaotic behavior could be found and analyzed in depth. Coupling might involve separate temperature and humidity profiles in the atmosphere itself (cf. Renno et al. 1994a, b), albedo changes at the surface — due to snow and ice cover or vegetation — and variable thermal inertia of the oceanic mixed layer or of soil moisture.

Acknowledgments. Jérôme Ballero helped with some of the initial calculations. Rong Fu, Sylvia George, David Randall, Nilton Renno and Graeme Stephens made constructive comments on earlier versions of the typescript or provided useful preprints and references. Yves Fouquart's suggestions as a reviewer greatly improve the paper, as did the feedback of various participants at the UCLA–University of Tokyo Workshops in 1993 and 1995. This work was sponsored by the European Commission and the French PNEDC (National Programme for the Study of Climate Dynamics: H. Le Treut and Z.X. Li), as well as the United States' NSF (National Science Foundation) Grant ATM95-23787 (M. Ghil and K. Ide). M. Ghil would also like to thank LMD's entire staff for their hospitality while occupying the Professorship of the Académie des Sciences at the Ecole Normale Supérieure. This is contribution number 4713 of UCLA's Institute of Geophysics and Planetary Physics.

Appendix

Jacobian matrices for sensitivity calculations

The derivative of $\vec{G}$ with respect to the longwave transmissivity $\vec{t}$ forms a rectangular matrix of $n+1$ rows and n columns:

$$\begin{aligned}(\frac{\partial \vec{G}}{\partial \vec{t}})_{ij} &= \frac{\partial G_i}{\partial t_j} = \frac{\partial}{\partial t_j}\sum_{l=0}^{l=n} k_{il}\sigma T_l^4 \\ &= \sum_{l=0}^{l=n} \sigma T_l^4 \frac{\partial k_{il}}{\partial t_j}, \quad i = 0, 1, ..., n, \quad j = 1, 2, ..., n.\end{aligned} \tag{A1}$$

With the expressions (8) giving the entries of $\mathbf{K}$, we can easily obtain the elements of the Jacobian matrix above. The formal differentiation distinguishes between three cases, $i<j$, $i=j$, and $i>j$:

$$\frac{\partial G_i}{\partial t_j} = \frac{k_{ij}}{t_j - 1}\sigma T_j^4 + \sum_{l=j+1}^{l=n} \frac{k_{il}}{t_j}\sigma T_l^4, \quad i = 0, 1, ..., n \ (i < j); \tag{A2}$$

$$\frac{\partial G_i}{\partial t_i} = \frac{\sum_{l=0}^{l=n} k_{il}\sigma T_l^4}{t_i - 1}, \quad i = 1, 2, ..., n; \tag{A3}$$

$$\frac{\partial G_i}{\partial t_j} = \frac{k_{ij}}{t_j - 1}\sigma T_j^4 + \sum_{l=0}^{l=j-1} \frac{k_{il}}{t_j}\sigma T_l^4, \quad i = 2, 3, ..., n \ (i > j). \tag{A4}$$

The derivative of $\vec{G}$ with respect to the shortwave transmissivity $\vec{\tau}$ also forms a rectangular matrix of $n+1$ rows and n columns:

$$(\frac{\partial \vec{G}}{\partial \vec{\tau}})_{ij} = \frac{\partial G_i}{\partial \tau_j} = \frac{\partial E_i}{\partial \tau_j}, \quad i = 0, 1, ..., n, \quad j = 1, 2, ..., n. \tag{A5}$$

With the expressions (9) defining $\vec{E}$, it is easy to get formulae for the elements of the Jacobian matrix in (A5). Again we distinguish three different cases:

$$\frac{\partial E_i}{\partial \tau_j} = \frac{E_i}{\tau_j}, \quad i = 0, 1, ..., n \ (i < j); \tag{A6}$$

$$\frac{\partial E_i}{\partial \tau_i} = (\prod_{l=i+1}^{l=n} \tau_l)[-1 + (1 - 2\tau_i)(\sum_{l=0}^{l=i-1} \rho_l \prod_{m=l+1}^{i-1} \tau_m^2)], \quad i = 1, 2, ..., n; \tag{A7}$$

$$\frac{\partial E_i}{\partial \tau_j} = (\prod_{l=i+1}^{l=n} \tau_l)(\tau_i - \tau_i^2)\{\sum_{l=0}^{l=j-1} [\rho_l \prod_{m=l+1}^{i-1} (\frac{2}{\tau_j}\tau_m^2)]\}, \quad i = 2, 3, ..., n \ (i > j) \tag{A8}$$

The derivative of $\vec{G}$ with respect to the shortwave reflectivity $\vec{\rho}$ forms a square $(n+1)$-by-$(n+1)$ matrix:

$$(\frac{\partial \vec{G}}{\partial \vec{\rho}})_{ij} = \frac{\partial G_i}{\partial \rho_j} = \frac{\partial E_i}{\partial \rho_j}, \quad i = 0, 1, ..., n, \quad j = 1, 2, ..., n. \tag{A9}$$

The entries of the matrix are:

$$\frac{\partial E_i}{\partial \rho_j} = 0, \quad i = 0, 1, ..., n \ (i < j); \tag{A10}$$

$$\frac{\partial E_i}{\partial \rho_i} = -\prod_{l=i+1}^{l=n} \tau_l, \quad i = 1, 2, ..., n; \tag{A11}$$

$$\frac{\partial E_i}{\partial \rho_j} = (\prod_{l=i+1}^{l=n} \tau_l)(\tau_i - \tau_i^2)(\prod_{m=j+1}^{m=i} \tau_m^2), \quad i = 2, 3, ..., n \ (i > j). \tag{A12}$$

Finally, the derivative of $\vec{G}$ with respect to the surface albedo ρ_0 forms a vector of $n+1$ elements:

$$(\frac{\partial \vec{G}}{\partial \rho_0})_i = \frac{\partial G_i}{\partial \rho_0} = \frac{\partial E_i}{\partial \rho_0}, \quad i = 0, 1, ..., n. \tag{A13}$$

Considering again the expression (9) of E_i yields

$$\frac{\partial E_0}{\partial \rho_0} = -\prod_{l=1}^{l=n} \tau_l, \tag{A14}$$

$$\frac{\partial E_i}{\partial \rho_0} = (\tau_i - \tau_i^2) \prod_{l=i+1}^{l=n} \tau_l \prod_{l=1}^{l=i-1} \tau_l^2, \quad i = 1, 2, ..., n. \tag{A15}$$

References:

Bony S, Duvel JP, Le Treut H (1995) Observed dependence of the water vapor and clear-sky greenhouse effect on sea surface temperature: Comparison with climate warming experiments. Climate Dynamics 11: 307-320

Budyko MI (1969) The effect of solar radiation variations on the climate of the Earth. Tellus 21: 611-619

Cess RD (1976) Climate change: An appraisal of atmospheric feedback mechanisms employing zonal climatology. J Atmos Sci 33: 1831-1843

Chalita S, Le Treut H (1994) Albedo of temperate and boreal forest and the Northern Hemisphere climate: a sensitivity experiment using the LMD GCM. Climate Dynamics 10: 231-240

Charlock TP, Sellers WD (1980) Aerosol effects on climate: Calculations with time-dependent and steady-state radiative-convective model. J Atmos Sci 37: 1327-1341

Crafoord C, Källén E (1978) A note on the condition for existence of more than one steady solution in Budyko-Sellers type models. J Atmos Sci 35: 1123-1125

Fouquart Y, Bonnel B (1980) Computations of solar heating of the Earth's atmosphere: A new parameterization. Beitr Phys Atmosph 53: 35-62

Ghil M (1976) Climate stability for a Sellers-type model. J Atmos Sci 33: 3-20

Ghil M (1984) Climate sensitivity, energy balance models and oscillatory climate models. J Geophys Res 89: 1280-1284

Ghil M, Childress S (1987) Topics in Geophysical Fluid Dynamics: Atmospheric Dynamics, Dynamo Theory and Climate Dynamics. Springer-Verlag, New-York, 485 pages

Ghil M, Le Treut H (1981) A climate model with cryodynamics and geodynamics. J Geophys Res 86: 5262-5270

Held IM, Suarez MJ (1974) Simple albedo feedback models of the icecaps. Tellus 36: 613-628

Held IM, Hemler RS, Ramaswamy V (1993) Radiative-convective equilibrium with explicit two-dimensional moist convection. J Atmos Sci 50: 3909-3927

Hu Q, Randall DA (1994) Low-frequency oscillations in radiative-convective systems. J Atmos Sci 51: 1089-1099

Källén E, Crafoord C, Ghil M (1979) Free oscillations in a climate model with ice-sheet dynamics. J Atmos Sci 36: 2292-2303

Le Treut H, Ghil M (1983) Orbital forcing, climatic interactions, and glaciation cycles. J Geophys Res 88C: 5167-5190

Manabe S, Strickler RF (1964) Thermal equilibrium of the atmosphere with a convective adjustment. J Atmos Sci 21: 361-385

Manabe S, Wetherald RT (1967) Thermal equilibrium of the atmosphere with a given distribution of relative humidity. J Atmos Sci 24: 241-259

Morcrette JJ (1991) Radiation and cloud radiative properties in the ECMWF operational weather forecast model. J Geophys Res 96D: 9121-9132

Nakajima S, Hayashi YY, Abe Y (1992) A study of the “runaway greenhouse effect” with a one-dimensional radiative-convective model. J Atmos Sci 49: 2256-2266

Nirenberg L (1981) Variational and topological methods in nonlinear problems. Bull. Amer. Math. Soc. (New Series), 4: 267-302

North GR (1975) Analytical solution to a simple climate model with diffusive heat transport. J Atmos Sci 32: 1301-1307

North GR, Howard L, Pollard D, Wielicki B (1979) Variational formulation of Budyko-Sellers climate models. J Atmos Sci 36: 255-259

North GR, Cahalan RF, Coakley JA, Jr. (1981) Energy balance climate models. Rev Geophys Space Phys 19: 91-121

Ramanathan V, Coakley JA (1978) Climate modeling through radiative convective models. Rev Geophys Space Phys 16: 465-489

Renno NO (1994) Multiple equilibria in radiative-convective atmospheres. In Proceedings of the AGU Fall Meeting, p 129, American Geophysical Union, Washington

Renno NO, Emanuel KA, Stone PH (1994a) A radiative-convective model with an explicit hydrological cycle, Part I: Formulation and sensitivity to model parameters. J Geophys Res 99D: 14429-14441

Renno NO, Stone PH, Emanuel KA (1994b) A radiative-convective model with an explicit hydrological cycle, Part II: Sensitivity to large changes in solar forcing. J Geophys Res 99D: 17001-17020

Sadourny R, Laval K (1984) January and July performance of the LMD general circulation model. In New Perspectives in Climate Modelling (Eds: Berger A, Nicolis C.), Elsevier Publishing Company, Amsterdam, pp 173-198

Saltzman B (1985) Paleoclimatic modeling. In Paleoclimate Analysis and Modeling (Ed: Hecht AD), John Wiley, New York, pp 341-396

Schlesinger ME, Mitchell JFB (1987) Climate model simulations of the equilibrium climatic response to increased carbon dioxide. Rev Geophys 25: 760-798

Schneider SH, Dickinson RE (1974) Climate modeling. Rev Geophys Space Phys 12: 447-493

Sellers WD (1969) A climate model based on the energy balance of the earth-atmosphere system. J Appl Meteorol 8: 392-400

Stephens GL, Webster PJ (1981) Clouds and climate: Sensitivity of simple systems. J Atmos Sci 38: 235-247

Table and Figure Captions

Table 1: Horizontally averaged variables from the LMD GCM, as used in the application of the present model to sensitivity calculations. Variables obtained from the GCM experiments: P – pressure (hPa), δP – layer thickness (hPa), T – temperature (K), q – water vapor (g/kg), O_3 – ozone concentration (cm.atm); derived optical properties (see text for details): t – longwave transmissivity, τ – shortwave transmissivity, ρ – shortwave reflectivity.

Table 2: Jacobian derivatives of equilibrium temperature $\vec{T}$ with respect to the atmospheric longwave (LW) transmissivity $\vec{t}$ ($\partial\vec{T}/\partial\vec{t}$, upper panel), to the atmospheric shortwave (SW) transmissivity $\vec{\tau}$ ($\partial\vec{T}/\partial\vec{\tau}$, middle panel), and to the atmospheric shortwave reflectivity $\vec{\rho}$ ($\partial\vec{T}/\partial\vec{\rho}$, lower panel). The temperature layer labels the columns and the parameter layer labels the rows in each panel. The units are degrees K.

Table 3: Derivative of the temperature in each layer with respect to surface albedo ρ_0, $\partial T_i/\partial\rho_0$. Units are degrees Kelvin.

Fig. 1: Schematic diagram of solar and terrestrial radiative fluxes; see text for symbols.

Fig. 2: Equilibrium temperature profiles for solar constant $S_0 = 1370$ W m^{-2}. The curves correspond to (a) the present climate with a surface albedo ρ_0=0.3; (b) a totally ice-covered Earth with ρ_0=0.9; and (c) the intermediate solution with ρ_0=0.525. The solid curve (GCM) corresponds to the GCM's horizontally averaged temperature profile.

Fig. 3: Vertical profile of model temperature change due to CO_2 doubling.

Fig. 4: Planetary albedo as a function of surface albedo, as used in EBMs (dotted) and in our RCM (solid).

Fig. 5: Relation between the outgoing longwave radiation (OLR) and the surface temperature from our one-dimensional RCM (solid). Two other curves are from zero-dimensional EBMs: Crafoord and Källén (1978: dotted) and North et al. (1981: dashed).

Fig. 6: Relation between the solar constant (normalized to the present value $S_0 = 1370\ \mathrm{Wm}^{-2}$) and the model surface temperature (K). The points a, b, and c correspond to the model's three equilibrium states for the present solar constant, $S/S_0 = 1$ (compare Fig. 2).

Fig. 7: Absorbed solar radiation (ASR: dashed) and OLR (solid) as a function of surface temperature. The OLR curve is identical to that shown in Fig. 5.

layer	P	δP	T	q	O_3	t	τ	ρ
11	15	44	223	0.006	1.59E-1	0.9630	0.9720	5.37E-3
10	73	69	204	0.009	3.92E-2	0.9765	0.9897	5.25E-3
9	152	101	205	0.010	1.67E-2	0.9486	0.9874	7.77E-3
8	274	132	222	0.063	7.41E-3	0.8468	0.9773	1.13E-2
7	416	150	242	0.393	3.38E-3	0.7255	0.9587	1.51E-2
6	573	151	257	1.292	1.65E-3	0.6633	0.9522	1.61E-2
5	718	134	268	2.747	8.44E-4	0.6428	0.9572	1.43E-2
4	841	104	276	5.285	4.43E-4	0.6163	0.9635	1.13E-2
3	926	69	281	7.739	2.28E-4	0.6578	0.9754	7.17E-3
2	980	39	285	8.857	1.11E-4	0.7756	0.9868	3.77E-3
1	1004	22	286	9.130	5.68E-5	0.8724	0.9930	1.98E-3

Table 1. Horizontally averaged variables from the LMD GCM, as used in the application of the present model to sensitivity calculations. Variables obtained from the GCM experiments: P − pressure (hPa), δP − layer thickness (hPa), T − temperature (K), q − water vapor (g/kg), O_3 − ozone concentration (cm.atm); derived optical properties (see text for details): t − longwave transmissivity, τ − shortwave transmissivity, ρ − shortwave reflectivity.

Layer (where LW t changes)

layer	**0**	**1**	**2**	**3**	**4**	**5**	**6**	**7**	**8**	**9**	**10**	**11**
11	-20	-23	-24	-26	-28	-31	-35	-40	-45	-46	-42	891
10	-19	-22	-23	-25	-27	-30	-34	-39	-43	-44	710	0
9	-20	-23	-24	-25	-27	-30	-34	-39	-44	152	0	0
8	-22	-25	-26	-27	-30	-33	-38	-43	16	0	0	0
7	-24	-28	-29	-30	-33	-37	-41	0	0	0	0	0
6	-24	-28	-29	-31	-34	-37	-5	0	0	0	0	0
5	-23	-27	-28	-30	-33	-7	0	0	0	0	0	0
4	-23	-27	-28	-29	-9	0	0	0	0	0	0	0
3	-21	-24	-25	-8	0	0	0	0	0	0	0	0
2	-18	-21	-4	0	0	0	0	0	0	0	0	0
1	-16	1	0	0	0	0	0	0	0	0	0	0

Layer (where SW τ changes)

layer	**0**	**1**	**2**	**3**	**4**	**5**	**6**	**7**	**8**	**9**	**10**	**11**
11	45	36	33	30	23	16	6	-5	-16	-18	-9	-1408
10	43	34	32	28	22	14	5	-6	-18	-20	-2809	-5
9	43	33	31	27	21	13	4	-8	-19	-1400	-15	-5
8	40	30	28	24	17	9	-1	-14	-448	-23	-15	-5
7	34	23	21	16	8	-1	-13	-217	-27	-22	-14	-5
6	25	12	9	3	-5	-16	-154	-28	-25	-21	-13	-4
5	13	-1	-4	-11	-21	-131	-30	-26	-24	-19	-13	-4
4	2	-14	-18	-25	-113	-33	-29	-25	-23	-18	-12	-4
3	-10	-27	-31	-118	-36	-32	-28	-24	-22	-18	-11	-4
2	-18	-37	-163	-39	-35	-31	-27	-24	-21	-17	-11	-4
1	-22	-260	-41	-38	-35	-31	-27	-23	-21	-17	-11	-4

Layer (where SW ρ changes)

layer	**0**	**1**	**2**	**3**	**4**	**5**	**6**	**7**	**8**	**9**	**10**	**11**
11	-27	-31	-32	-34	-37	-41	-47	-53	-60	-61	-56	-1161
10	-26	-30	-31	-33	-36	-40	-45	-52	-59	-60	-2280	-10
9	-27	-31	-32	-34	-37	-41	-46	-53	-60	-1159	-30	-10
8	-29	-33	-34	-36	-40	-44	-50	-57	-399	-46	-30	-10
7	-33	-38	-40	-42	-46	-51	-58	-214	-54	-44	-28	-9
6	-39	-45	-47	-49	-54	-60	-164	-55	-49	-40	-26	-9
5	-45	-52	-53	-57	-62	-144	-57	-50	-45	-36	-24	-8
4	-51	-59	-61	-64	-129	-60	-52	-45	-41	-33	-22	-7
3	-56	-65	-67	-132	-63	-56	-49	-42	-38	-31	-20	-7
2	-60	-70	-165	-66	-60	-53	-46	-40	-36	-29	-19	-6
1	-62	-239	-69	-65	-58	-52	-45	-39	-35	-29	-19	-6

Layer (where temperature changes)

Table 2. Jacobian derivatives of equilibrium temperature $\vec{T}$ with respect to the atmospheric longwave (LW) transmissivity $\vec{t}$ ($\partial\vec{T}/\partial\vec{t}$, upper panel), to the atmospheric shortwave (SW) transmissivity $\vec{\tau}$ ($\partial\vec{T}/\partial\vec{\tau}$, middle panel), and to the atmospheric shortwave reflectivity $\vec{\rho}$ ($\partial\vec{T}/\partial\vec{\rho}$, lower panel). The temperature layer labels the columns and the parameter layer labels the rows in each panel. The units are degrees K.

layer	**0**	**1**	**2**	**3**	**4**	**5**	**6**	**7**	**8**	**9**	**10**	**11**
$\partial\vec{T}/\partial\rho_0$	-82	-70	-68	-64	-58	-51	-44	-39	-35	-28	-18	-6

Table 3. Derivative of the temperature in each layer with respect to surface albedo ρ_0, $\partial T_i/\partial\rho_0$. Units are degrees Kelvin.

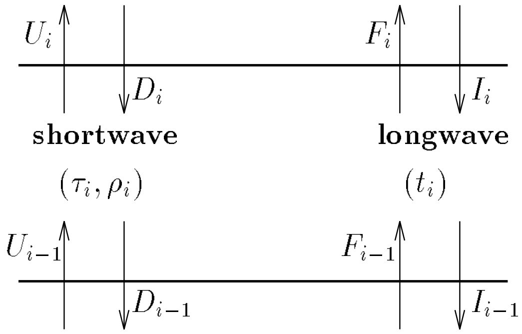

Fig. 1. Schematic diagram of solar and terrestrial radiative fluxes; see text for symbols.

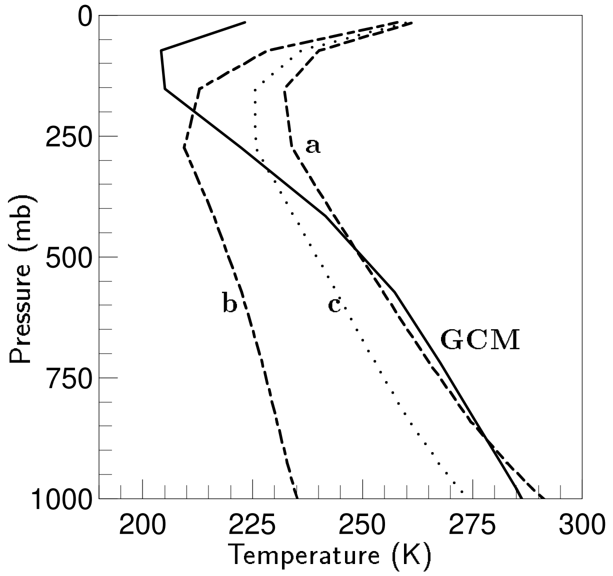

Fig. 2. Equilibrium temperature profiles for solar constant $S_0 = 1370$ W m^{-2}. The curves correspond to (a) the present climate with a surface albedo ρ_0=0.3; (b) a totally ice-covered Earth with ρ_0=0.9; and (c) the intermediate solution with ρ_0=0.525. The solid curve (GCM) corresponds to the GCM's horizontally averaged temperature profile.

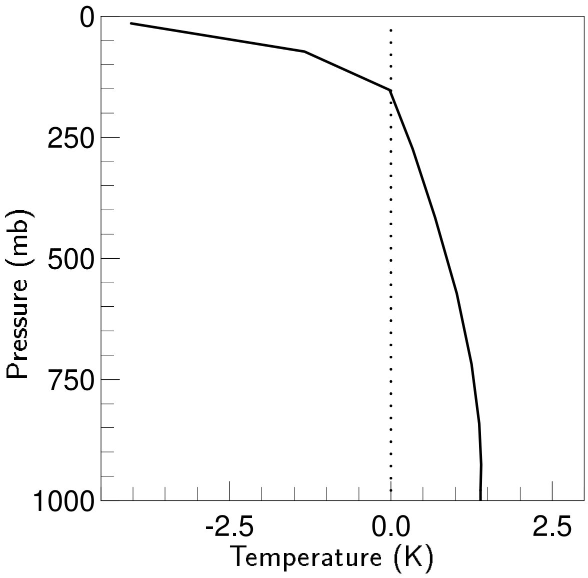

Fig. 3. Vertical profile of model temperature change due to CO_2 doubling.

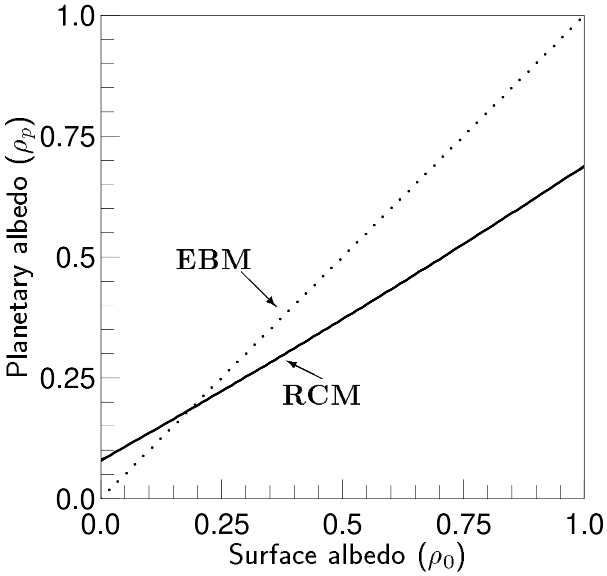

Fig. 4. Planetary albedo as a function of surface albedo, as used in EBMs (dotted) and in our RCM (solid).

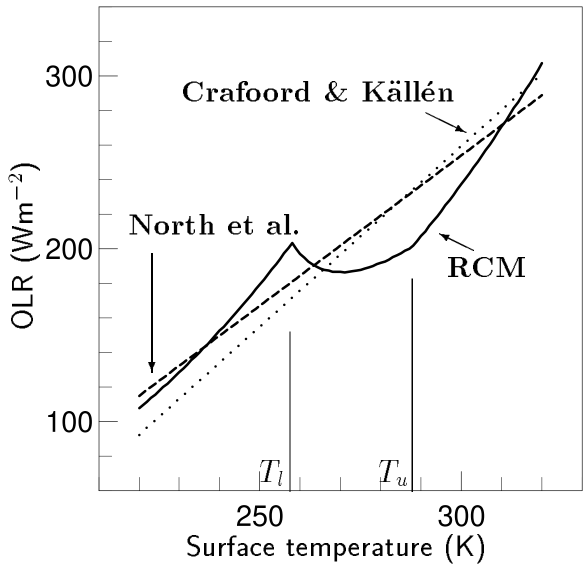

Fig. 5. Relation between the outgoing longwave radiation (OLR) and the surface temperature from our one-dimensional RCM (solid). Two other curves are from zero-dimensional EBMs: Crafoord and Källén (1978: dotted) and North et al. (1981: dashed).

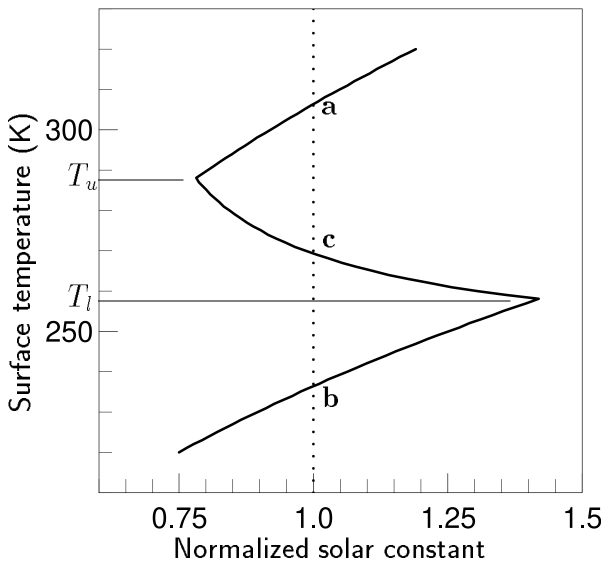

Fig. 6. Relation between the solar constant (normalized to the present value $S_0 = 1370\ \mathrm{Wm}^{-2}$) and the model surface temperature (K). The points a, b, and c correspond to the model's three equilibrium states for the present solar constant, $S/S_0 = 1$ (compare Fig. 2).

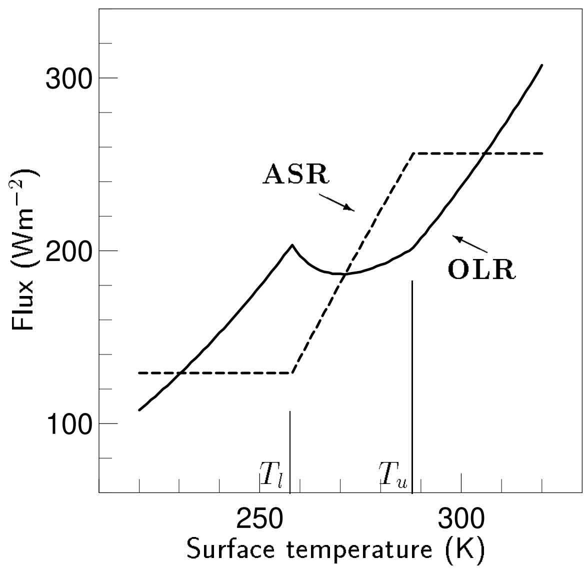

Fig. 7. Absorbed solar radiation (ASR: dashed) and OLR (solid) as a function of surface temperature. The OLR curve is identical to that shown in Fig. 5.